SUPPLEMENTARY INFORMATION

Demonstration of Feasibility of X-Ray Free Electron Laser Studies of Dynamics of Nanoparticles in Entangled Polymer Melts

Jerome Carnis[1], Wonsuk Cha[1], James Wingert[2], Jinback Kang[1], Zhang Jiang[3], Sanghoon Song[4], Marcin Sikorski[4], Aymeric Robert[4], Christian Gutt[5,6,7], San-Wen Chen[2], Yeling Dai[2], Yicong Ma[2], Hongyu Guo[2], Laurence B. Lurio[8], Oleg Shpyrko[2], Suresh Narayanan[3], Mengmeng Cui[9], Irem Kosif[9], Todd Emrick[9], Thomas P. Russell[9], Hae Cheol Lee[10], Chung-Jong Yu[10], Gerhard Grübel[5,6], Sunil K. Sinha[2], Hyunjung Kim[1,*]

[1] Department of Physics, Sogang University, Seoul 121-742, Korea
[2] Department of Physics, University of California, San Diego, CA 92093, USA
[3] Advanced Photon Source, Argonne National Laboratory, Argonne, IL 60439, USA
[4] LCLS, SLAC National Accelerator Laboratory, Menlo Park, CA 94025, USA
[5] Deutsches Elektronen-Synchrotron (DESY), Notkestraße 85, D-22607 Hamburg, Germany
[6] Center of Ultrafast Imaging, Luruper Chaussee 149, 22761 Hamburg, Germany
[7] Department of Physik, University of Siegen, D-57068 Siegen, Germany
[8] Department of Physics, Northern Illinois University, De Kalb, IL 60115, USA
[9] Polymer Science and Engineering Department, University of Massachusetts, Amherst, MA 01003, USA
[10] Pohang Accelerator Laboratory, Pohang, Gyeongbuk 790-784, Korea

*Correspondence to hkim@sogang.ac.kr

1. Spatial correlation analysis

The speckle size can be directly related to the full width at half maximum (FWHM) of the spatial intensity autocorrelation given by[S1]

$$C(\Delta r) = \frac{\left\langle \bar{I}(r) \times \bar{I}(r+\Delta r) \right\rangle}{\left\langle I \right\rangle^2} \quad ,$$

where Δr represents the distance in pixels and $\bar{I}(r)$ an average intensity over pixels with an identical wave vector transfer q. Since the beam is expected to be asymmetric, as measured with knife edge scans (4.7μm×3.3μm (H×V)), the analysis is applied to the horizontal and vertical directions separately. The sample consists of gold nanoparticles dispersed in a polystyrene matrix at 393K. It is important to note that the spatial correlation tends to $1+\beta$ as Δr goes to 0, where β is the speckle contrast. Since the self-correlation term at Δr = 0 includes a dominant contribution from Poisson noise in photon statistics[S1,S2]and the correlation at Δr = 1 includes the contribution of photon sharing between detector pixels, an estimation of the contrast can be made by cross-correlating two frames temporally close (sufficiently close to neglect sample dynamics) and taking the point at Δr = 0. Because the contrast between frames will be slightly lower that the self-contrast, this method gives also a high-limit for the FWHM of the curves. Only frames with sufficient scattering intensity are used. Spatial cross-correlations are calculated in a square area of 50×50 pixels centered at q=0.0038Å^{-1} as shown with a yellow box in Fig. S1 (a), between consecutives frames separated by ~7s, much smaller than the typical relaxation time ~10^3s measured for this data set (see Fig. 4 a). Correlations are averaged along q within each frame and then averaged over the total number of frames. A small area of the speckle pattern averaged over 150 frames for better visualization is presented in (b). A particular cross-correlation pattern calculated between two consecutive frames is plotted in (c). Average line cuts in the horizontal and vertical directions as a function of Δr are presented in (d). When Δr is larger than the speckle size, the spatial correlation approaches 1 since there is no more correlation between the intensities. A slight deviation from 1 is typically due to the limited number of speckles in the selected area for the calculation, leading to variations in <I>.

The contrast and beam sizes calculated from the speckle size in both directions are summarized in the Table S1. The contrast is slightly lower than those obtained from XPCS analysis ($g_2(0) \approx 0.08$-0.10 as displayed in Fig. S4) due to the cross-correlation scheme. The

beam size d_{beam} is estimated from the speckle size $d_{speckle}$ using $d_{beam} \approx \frac{\lambda \times SDD}{d_{speckle}}$, where SDD is the sample to detector distance and λ the wavelength. The estimation from 100 pulses yields an average beam size of 3.5μm×3.5μm (H×V), whereas 4.7μm×3.3μm (H×V) obtained by knife edges scans. It is worth emphasizing that the determination of the beam size via speckle size is intrinsically more precise than knife edge scans, which suffer mainly from positional jitter and profile fluctuation of LCLS beam.

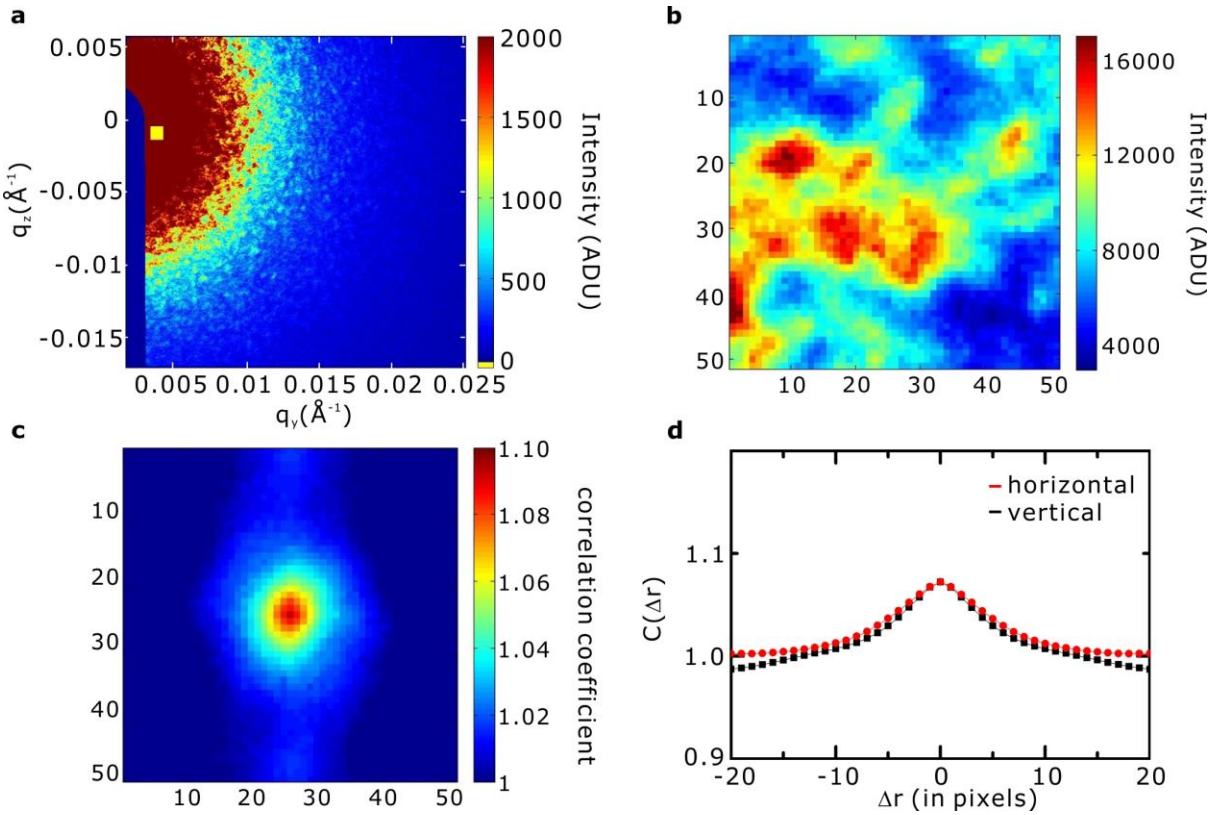

Figure S1. Spatial correlation analysis. a. Scattering pattern from the sample for 100 pulses per frame averaged over 150 frames. The yellow box is centered at q=0.0038Å^{-1}. The dark blue feature on the left is the beamstop. **b.** The detailed speckle pattern from the yellow box in **a.** The mean intensity in that area is 4.72 photons per pixel. **c.** A particular cross-correlation pattern calculated between two consecutive frames**. d**. Average line cuts at the maximum in intensity. The correlation was calculated both in the horizontal (in red) and vertical (in black) directions. Lines between data points are a guide for the eye.

Table S1. The contrast and the speckle size obtained from FWHMs in Fig. S1 (d). Error bars correspond to the standard deviation of the averaged ensemble.

	Contrast	Speckle FWHM (pixels)	Calculated beam size (μm)	Knife edge scans (μm)
Horizontal	0.07 ± 0.01	10.3 ± 0.6	3.5 (3.3 - 3.7)	4.7
Vertical	0.07 ± 0.01	10.4 ± 0.8	3.5 (3.2 - 3.7)	3.3

2. Intensity distribution analysis

For a fully coherent beam a single transverse mode is present in the beam. For partially coherent beam the integrated intensity distribution is described by the negative binomial distribution with a parameter *M*, corresponding to the number of modes[S3]

$$P(I) = \frac{\Gamma(I+M)}{\Gamma(I+1)\Gamma(M)}\left(1+\frac{M}{<I>}\right)^{-I}(1+\frac{<I>}{M})^{-M}.$$

The contrast is related to the number of modes via β=1/*M*.

Here the negative binomial distribution has been extended to a continuous intensity distribution. This analysis is valid if the mean intensity per pixel is large enough (several photons per pixel) to neglect the effect of Poisson noise in photon statistics[S4]. With very low scattering intensities one has to apply methods such as the droplet algorithm[S1,S5] in order to identify individual photon events. A typical fitting for one frame containing the sum of 100 pulses is shown in Fig. S2(a). The evolution of the number of modes *M* during the full run with 100 pulses per frame is presented in (b). The mean number of mode is $<M_{fit}>=12.7\pm4.4$, thus corresponding to a contrast of ~0.08. It is in good agreement with the contrast obtained from XPCS analysis.

Following Ref. S6, we now introduce the photocount degeneracy parameter $\delta_c = \frac{\langle I \rangle}{M}$ extended to continuous intensity distributions. It can be shown that for large δ_c the negative binomial distribution tends to the gamma density function:

$$P(I) = \left(\frac{M}{<I>}\right)^{M}\frac{I^{M-1}e^{-M\frac{I}{<I>}}}{\Gamma(M)}$$

The fitting of the intensity distribution histogram is presented in Fig. S3. Although the fitting seems reasonable, the number of modes obtained is not in agreement with the one obtained from XPCS analysis, indicating that we are in an intermediate intensity regime with $\delta_c \approx 0.5$ where the gamma density function cannot be used.

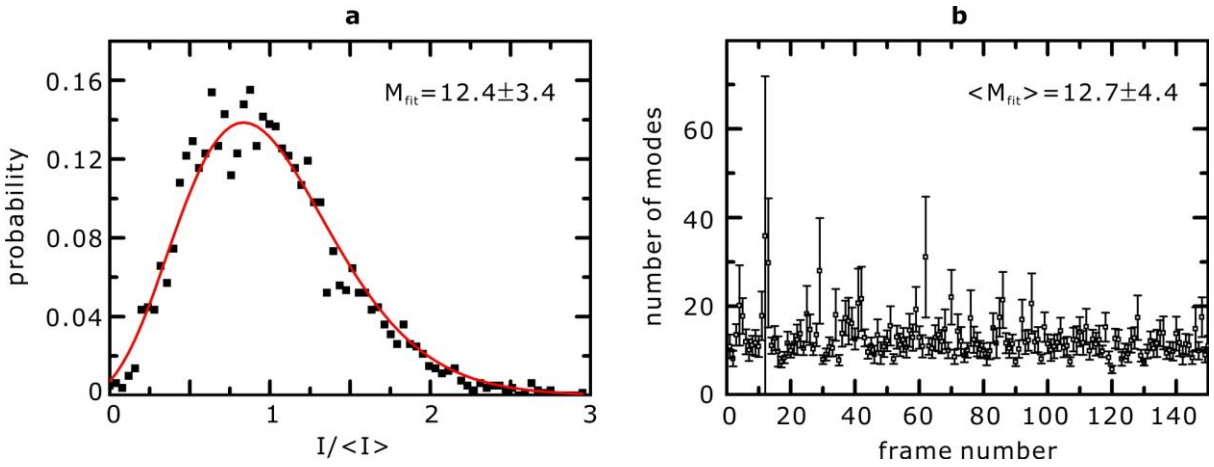

Figure S2: Intensity distribution and its fit to the negative binomial distribution. a. Intensity distribution histogram (symbol) and its fit to the negative binomial distribution (solid line) for a particular frame with 100 pulses. Pixels in a small region of interest centered on q=0.0032A^{-1} with a width of 0.0002A^{-1} were used for the calculation. There were 5.95 photons per pixel on average. The fit yields the number of modes M_{fit} in the particular q range. In **b** the evolution of the number of modes during a measurement of a total 150 frames is plotted. Error bars represent the 95% confidence interval. The average number of modes in both cases is larger than the ideal M=1 for a single pulse per frame.

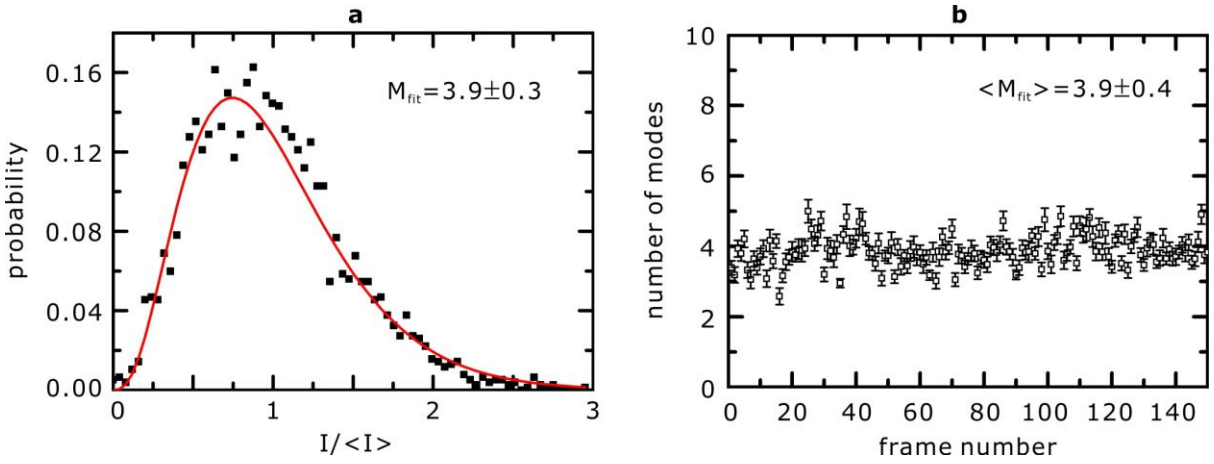

Figure S3: Intensity distribution and its fit to the gamma density function. a. The same data as Fig. S2 was used. In **b** the evolution of the number of modes during a measurement of a total 150 frames is plotted. The average number of modes M_{fit} is not in agreement with XPCS results.

3. Aging effect at different wave vector transfers

In Fig. S4, intensity autocorrelation functions g_2 are shown for various wave vector transfers (extended from Fig. 3) calculated from the first 8.5 min. (shown in red) and the last 8.5 min (in blue), i.e., first and last 75 frames among a total of 150 frames, in (a) at 103 min. and in (b) at 477 min. after the temperature reaching equilibrium at 393K. The corresponding decay time constants are presented in Table S2.

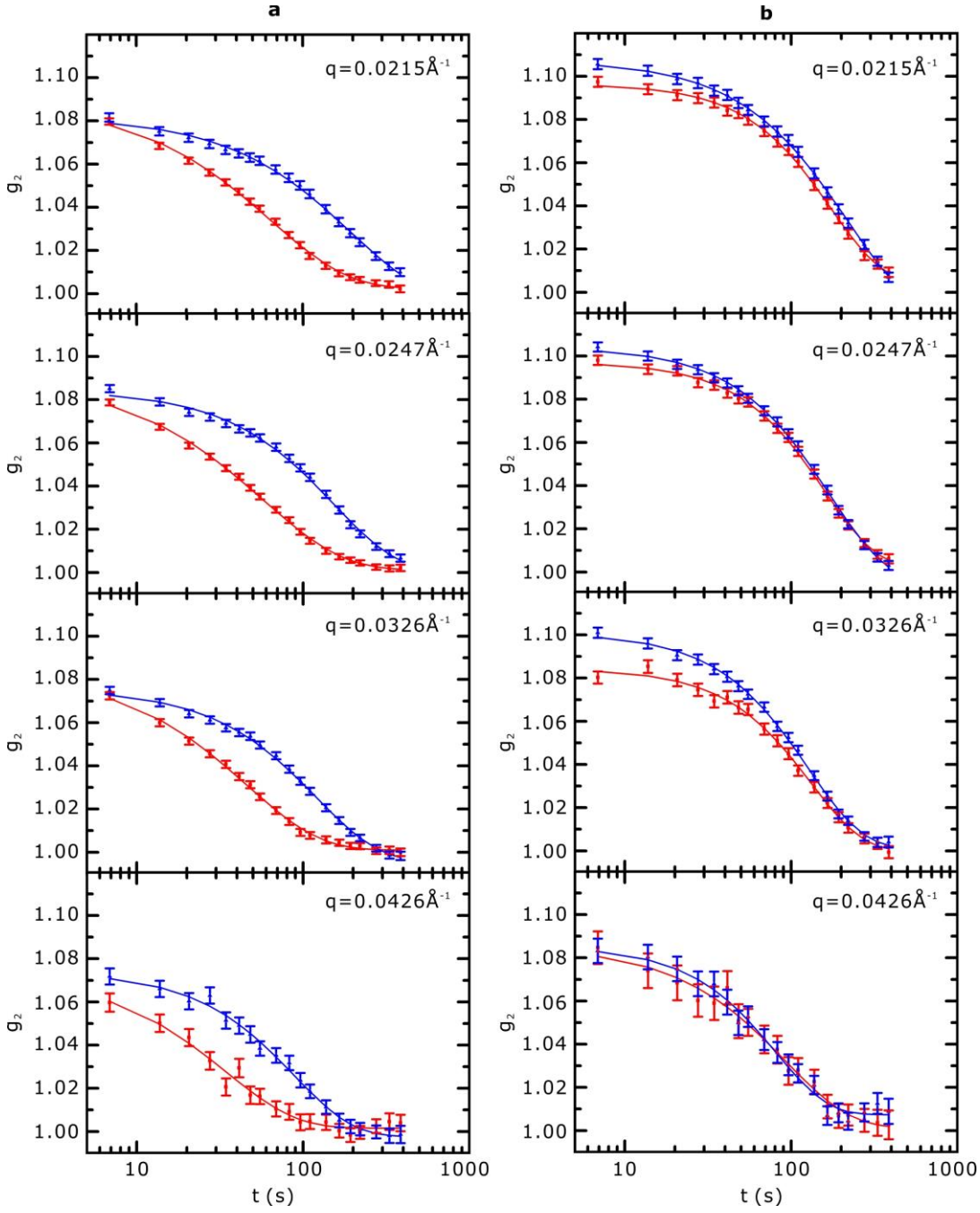

Figure S4. Comparison of g_2 functions at two different ages for various wave vector transfers. g_2 functions are calculated from the first 75 frames (in red) and from the last 75 frames (in blue) among a total 150 frames

Table S2. Relaxation time constants at different wave vector transfer at different ages. Time constants extracted from the fits of g_2 functions in Fig.S3 are summarized.

q (Å $^{-1}$)	103min		477min	
	First 8.5min	Last 8.5min	First 8.5min	Last 8.5min
0.0215	140s	353s	300s	333s
0.0247	123s	267s	252s	284s
0.0326	92s	181s	206s	216s
0.0426	83s	168s	174s	145s

4. Transmission coefficients of optical components

The transmission coefficients of all the optical components in the XCS instrument starting from the exit of the undulator are shown in Table S3 for calculating the average number of photons incident on the sample position.

Table S3. Transmission coefficients of the beamline optical components at the XCS instrument at LCLS. Transmission coefficients of the optical components at the XCS instrument at 8.7keV used in the calculation for the flux incident on the sample.

Component	Transmission coefficient
Intensity monitor (two of them)	0.975
Compound refractive lenses	0.263
Exit diamond window	0.888
Monochromator	0.02
Hard X-ray Offset Mirrors	0.6
Kapton window	0.963
Total	2.57×10^{-3}

5. Estimation for energy deposition on a gold nanoparticle

Multiplying the nominal averaged number of photons (9.2×10^{11} photons/pulse) by the transmission coefficient of the beamline optics (2.57×10^{-3}, as indicated in Table S3) and dividing by the beam size 3.5μm×3.5μm (H×V) deduced from the speckle size, we obtain an average incident photon density of 1.93×10^{16} photons/pulse/cm^2. The absorption cross section of a 5.5nm diameter gold nanoparticle (mass absorption coefficient 166.9cm^2/g, density 19.3g/cm^3) is σ_{abs}=2.8061×10^{-16}cm^2. Thus by multiplying it by the incident photon density calculated previously gives ~5.41 photons absorbed by nanoparticles. Assuming that the electronic excitation is completely converted into heat energy for each atom and using the specific heat of gold (129.1J/kg·K) and dividing by the number of atoms in the nanoparticle, we can get the average heating for each atom in the nanoparticle $\Delta T\sim3.5\times10^4$K/atom.

6. References

S1. DeCaro, C. *et al*. X-Ray speckle visibility spectroscopy in the single-photon limit. *J. Synchrotron Rad*. **20**, 332-338 (2012).

S2. Tsui, O. K. C., Mochrie, S. G. J. and Berman, L. E. Statistical Analysis of X-Ray Speckle at the NSLS. *J. Synchrotron Rad*. **5**, 30-36 (1998).

S3. Goodman, J. *Speckle Phenomena in Optics: Theory and Application*. (Roberts & Company Publishers, Greenwood Village, 2007).

S4. Dufresne, E., Bruning, R., Sutton, M., Rodricks, B. and Stephenson, G.B. A statistical technique for characterizing X-ray position-sensitive detectors. *Nucl. Instrum. Meth Phys. Res. A* **364**, 380 (1995).

S5. Hruszkewycz, S.O. *et al*. High Contrast X-ray Speckle from Atomic-Scale order in Liquids and Glasses. *Phys. Rev. Lett*. **109**, 185502 (2012).

S6. Saldin,E. L., Schneidmiller, E. A. and Yurkov, M.V. Statistical properties of radiation from VUV and X-ray free electron laser. *Opt. Commun.* **148**, 383 (1998).